New Concepts for Assessing Global Organ Function and Disease Activity Based on Combined PET and Structural Imaging Techniques

Sandip Basu, MD[a], Habib Zaidi, PhD, PD[b], Abass Alavi, MD[a],*

- Concept of global metabolic activity
- Applications of global metabolic activity in neurology
- Assessment of global metabolic activity of atherosclerosis (Athero-Burden) by combined FDG-PET and CT imaging
- Application of global metabolic activity to diffuse hepatic steatosis
- Application of global metabolic activity in oncology
- Advances in medical image segmentation within the context of quantitative PET imaging
- Principle of partial volume correction of standardized uptake value for the purpose of calculating global metabolic activity
- Summary
- References

In this paper, we explore the current state and the future prospects for assessing regional versus global function by combining volumetric data from tomographic structural imaging techniques such as CT/MR imaging and quantitative metabolic information provided by functional modalities such as PET. The principle for calculating global metabolic activity is based on multiplying partial volume-corrected average standardized uptake value to the volume of the organ of interest generated from the CT/MR image. With the introduction of fusion imaging into the daily practice of medicine, we believe that a quantitative approach using data from both structural and functional modalities will be the way forward for accurate assessment of various pathophysiological states. Medical image segmentation is an integral part of this promising approach. This involves the identification of specific tissues of interest in a given structural image, which allows measuring regional functional parameters of an individual component within an organ. The future impact of this approach is discussed along with a brief overview of the concepts that allow for segmentation of different organs. The major direct impact of these novel quantitative techniques will include monitoring therapeutic efficacy in various malignancies. Incorporation or substitution of such quantitative ^{18}F-Fluorodeoxyglucose (FDG)-PET

doi:10.1016/j.cpet.2007.10.001

data into the different tumor response schemes used in clinical oncology trials like the World Health Organization (WHO) criteria, the Southwest Oncology Group (SWOG) criteria, or the Response Evaluation Criteria in Solid Tumors (RECIST) may substantially improve our ability to evaluate the efficacy of therapies. While the major utility of such measurements will be more accurate assessment of disease activity in cancer, measurement of global metabolic activity in various neuropsychiatric disorders and quantification of the extent of atherosclerosis may influence the management of patients with these disorders.

This paper is intended to discuss ways in which global and regional organ function may be assessed using advanced imaging technologies. In addition, we discuss using FDG-PET to monitor treatment response in various tumors as well as quantification of tumor burden in the entire body. Special emphasis is put on FDG as a model that can also be adopted for other PET radiotracers. The merits of advanced quantitative measures for disease activity assessment in cancer and other disorders will also be addressed.

Concept of global metabolic activity

The idea of measuring global metabolic activity was first introduced by Alavi and colleagues [1] in studies of glucose metabolism of the brain in patients with Alzheimer's disease (AD) and in age-matched controls. The measured mean cerebral metabolic rates for glucose were multiplied by segmented brain volumes as seen on MR images. By employing this approach, these investigators were able to demonstrate significant differences between these two populations compared with conventional techniques. The same investigators have proposed adopting a similar approach for assessing global normal organ function and overall disease activity in other settings.

This concept requires calculating tissue volume by using modern computer-based algorithms and accurate (partial volume corrected) measurement of regional metabolic activity (or other functional process) of the organ or disease site of interest. Partial volume effect (PVE) is an important limiting factor for accurate quantitation of radiotracer concentration with PET. However, with recent advances, it is possible to correct for PVEs of the relatively low spatial resolution functional imaging techniques (see the article by Rousset and colleagues elsewhere in this issue). By multiplying partial volume-corrected metabolic measures (such as standardized uptake value [SUV], rates of metabolism, and so forth) by volumetric measures from structural images, one can calculate the metabolic volumetric product (MVP) for the organ of interest or the diseased site. In situations with multiple disease sites such as metastatic cancer, by combining these measurements in the entire body, it is feasible to calculate the global metabolic activity of the underlying process.

The power of this concept stems from its ability to use both structural and functional alterations that take place as a consequence of disease states such as cancer or of a normal process such as aging. By now, it is well documented that the results from existing uni-dimensional measurement (RECIST) criteria, a standard region of interest (ROI)-based SUV estimate, or other semiquantitative measurements are often prone to inaccuracy and high variability [2]. The concept of global metabolic activity has significant implications for the assessment of cancer and evaluating cancer treatment. It is important in testing new therapeutic agents, and can be effectively employed in the management of other conditions such as atherosclerosis, cardiac disorders, and central nervous system diseases. We provide examples of some of the practical uses of this concept and data generated from preliminary experiments in our own laboratory.

Applications of global metabolic activity in neurology

In AD, Alavi and colleagues [1] hypothesized that the absolute amount of glucose used by the entire brain would prove to be a more reliable indicator of the reduced cognitive function than metabolic rates calculated for a unit of brain volume alone. They investigated 20 patients with the probable diagnosis of AD and 17 age-matched controls who underwent FDG-PET and MR imaging within a short time interval. The uncorrected cerebral metabolic rate for glucose (CMRGlc) values were atrophy corrected using the following equation:

$$\text{Atrophy corrected average CMRGlc} = \frac{\text{Mean CMRGlc}}{\text{percentage of brain tissue in the intracranial volume}}$$

(1)

Absolute whole brain metabolism was calculated by using the formula:

$$\text{Absolute whole brain metabolism} = \text{Atrophy corrected mean CMRGlc} \times \text{brain volume}$$

(2)

Average metabolic rates, when corrected for atrophy, were 3.91 ± 1.02 and 4.43 ± 0.87 (mg of glucose per 100 cm^3 brain tissue per minute) for AD patients and controls, respectively, and the difference was not statistically significant (Table 1). Atrophy-weighted

Table 1: Whole brain PET data for Alzheimer's disease and controls

	CMRGlc (uncorrected), mean ± SD	CMRGlc (corrected), mean ± SD	Atrophy-weighted total-brain metabolism, mean ± SD	Absolute whole-brain metabolism, mean ± SD
AD patients	3.15 ± 0.83[a]	3.91 ± 1.02[b]	29.96 ± 7.90[c]	37.24 ± 9.65[d]
Controls	3.83 ± 0.70	4.43 ± 0.87	39.09 ± 7.02	45.09 ± 8.52

CMRGlc in mg glucose/100 cc/brain tissue/min; Atrophy-weighted total-brain metabolism in mg glucose/brain/min; Absolute whole-brain metabolism; Absolute whole-brain metabolism in mg glucose/brain/min.
Abbreviations: AD, Alzheimer's disease; CMRGlc, cerebral metabolic rate for glucose.
[a] Significantly different from controls $P = .01$.
[b] Not Significantly different from controls $P = .11$.
[c] Significantly different from controls $P = .0008$.
[d] Significantly different from controls $P = .014$.
(*Adapted from* Alavi A, Newberg AB, Souder E, et al. Quantitative analysis of PET and MRI data in normal aging and Alzheimer's disease: atrophy weighted total brain metabolism and absolute whole brain metabolism as reliable discriminators. J Nucl Med 1993;34:1684; with permission.)

total brain metabolism (calculated by multiplying the brain volume, as measured by MR image analysis, by the average metabolic rate) and absolute whole brain metabolism (calculated by multiplying the brain volume by the average metabolic rate corrected for atrophy) were also assessed. Atrophy-weighted total brain metabolism was significantly different between the two groups (29.96 ± 7.90 for AD patients compared with 39.1 ± 7.0 for controls, $P < .001$), and it also correlated with Mini-Mental State Examination (MMSE) scores (r = 0.59, $P < .01$). Absolute whole brain metabolism was also found to be significantly different between AD and control groups and correlated well with MMSE scores. These data demonstrated that although the metabolic rate per unit weight of the remaining brain is unchanged in AD compared with controls, atrophy-weighted total brain metabolism and absolute whole brain metabolism are significantly affected. They concluded that both indices could prove to be sensitive correlates for cognitive dysfunction in AD (see Tables 1 and 2).

Assessment of global metabolic activity of atherosclerosis (Athero-Burden) by combined FDG-PET and CT imaging

This method was employed to quantify the extent of atherosclerosis in the aorta by multiplying SUVs measured at different segments in the aortic wall with aortic wall volumetric data provided by CT to yield MVPs. Bural and colleagues [3] used this approach in 18 patients who had both FDG-PET and contrast-enhanced CT of the chest and abdomen. All had homogeneous diffuse FDG uptake in all segments of the aortic wall. The patients were divided into three groups according to their age. FDG uptake was measured in different segments of the aorta by calculating the mean SUV for each segment. On each axial CT image, ROI tracings along the inner and outer wall contours of the

Table 2: Recovered whole brain PET data for AD and controls

	Recovered CMRGlc (uncorrected), mean ± SD	CMRGlc (corrected), mean ± SD	Atrophy-weighted total-brain metabolism, mean ± SD	Absolute whole-brain metabolism, mean ± SD
AD patients	4.89 ± 1.22[a]	6.06 ± 1.48[b]	46.61 ± 12.24[c]	57.86 ± 14.89[d]
Controls	5.38 ± 0.88	6.22 ± 1.07	55.23 ± 9.82	63.73 ± 10.07

CMRGlc in mg glucose/100 cc/brain tissue/min; Atrophy-weighted total-brain metabolism in mg glucose/brain/min; Absolute whole-brain metabolism; Absolute whole-brain metabolism in mg glucose/brain/min.
Abbreviations: AD, Alzheimer's disease; CMRGlc, cerebral metabolic rate for glucose.
[a] Not Significantly different from controls $P = .17$.
[b] Not Significantly different from controls $P = .72$.
[c] Significantly different from controls $P = .026$.
[d] Significantly different from controls $P = .18$.
(*Adapted from* Alavi A, Newberg AB, Souder E, et al. Quantitative analysis of PET and MRI data in normal aging and Alzheimer's disease: atrophy weighted total brain metabolism and absolute whole brain metabolism as reliable discriminators. J Nucl Med 1993;34:1685; with permission.)

aorta were generated. The inner surface area was subtracted from the outer surface area, and net area values for each segment were subsequently multiplied by slice thickness to calculate aortic wall volume. The atherosclerotic burden (AB) was calculated for each segment of the aorta by multiplying SUV by the wall volume. When the aortic wall volumes, SUVs, and AB values in each aortic segment for each age group were compared, they were found to increase with age ($P < .05$) (Table 3 and Fig. 1).

Application of global metabolic activity to diffuse hepatic steatosis

Bural and colleagues employed combined FDG-PET and MR imaging to calculate hepatic MVPs in both healthy subjects and subjects with diffuse hepatic steatosis. They investigated 24 subjects in this study (11 men, 13 women, age range 21 to 75 years). All subjects had FDG-PET and MR scans within a time interval of 52 ± 60 days. Twelve of the 24 subjects had diffuse hepatic steatosis based on MR imaging criteria. The remaining 12 were selected as age-matched controls, as they had normal-appearing livers on MR images and on FDG-PET scans. They calculated the mean and maximum hepatic SUVs for every subject from the FDG-PET images. They also calculated the volume of the liver for each subject from MR images by summing the surface area values and multiplying by the slice thickness. Subsequently, the hepatic MVP was calculated by multiplying liver volume by the mean hepatic SUV in each subject. The mean and maximum hepatic SUVs and the hepatic MVPs were compared for two groups. Mean and maximum hepatic SUVs for the group with diffuse hepatic steatosis were 2.2 ± 0.1 and 3.2 ± 0.4, respectively, compared with 1.8 ± 0.2 and 2.4 ± 0.3 for the control group, respectively, and all were statistically significantly different ($P < .05$). Hepatic MVP was 3.7 ± 0.2 (SUV - L) for the group with diffuse hepatic steatosis, and 2.3 ± 0.9 (SUV - L) for the control group ($P < .05$).

Application of global metabolic activity in oncology

The concept of whole-body metabolic burden (WBMB) was examined by investigators from the University of Pennsylvania in lymphoma patients. Individual lesion metabolic burden (MB) was calculated by measuring the volume on CT (V_{CT}), the mean SUV measured on PET of the CT volume (SUV_{meanCT}), and the Recovery Coefficient (RC):

$$MB = SUV_{meanCT} (V_{CT})/RC \qquad (3)$$

where RC recovers counts that extend beyond the CT volume as a result of partial volume effects, and was obtained from a calibration plot study of hot sphere activity within a warm background phantom for the PET scanner used. For lesions larger than 3 cm, RC was 1. The preliminary results showed that MB is a promising measure when corrected for partial volume effects and operator error in drawing ROIs. The WBMB was defined as the sum of the individual MB of all lesions identified. This index appeared promising to monitor changes in total body tumor burden in patients undergoing treatment.

$WBMB = \sum_{i=1}^{n} MB_i$ where n is the number of individual tumors outlined. Akin to single-lesion MB, the WBMB had units of SUV $\times$ volume. Examples of this have been depicted in Table 4.

More recently, Larson and colleagues [4] reported the concept of "Total Lesion Glycolysis" (TLG), which was defined as $TLG = SUV_{mean} \times volume\ of\ PET\ lesion$. They further defined the response index (also known as Larson-Ginsberg Index − LGI) as:

$$\Delta TLG\ (LGI) =$$
$$\frac{\left[(SUV_{mean})_1 \times (Vol)_1 - (SUV_{mean})_2 \times (Vol)_2\right]}{(SUV_{mean})_1 \times (Vol)_1} \times 100$$
$$(4)$$

where "1" and "2" denote the pre- and posttreatment FDG-PET scans, respectively. They investigated 41 patients with locally advanced lung ($n = 2$), rectal ($n = 17$), esophageal ($n = 16$), and gastric

---

Table 3: **SUVs (mean ± SD) for each aortic segment and for the total aorta**

Age, y	Ascending aorta	Arch of the aorta	Descending thoracic aorta	Abdominal aorta	Total SUV
21–40 ($n = 5$)	1.7 ± 0.3	1.8 ± 0.3	1.7 ± 0.3	1.6 ± 0.3	1.7 ± 0.3
41–60 ($n = 7$)	2.0 ± 0.4	1.9 ± 0.5	2.1 ± 0.5	1.8 ± 0.2	2.0 ± 0.4
61–80 ($n = 6$)	2.3 ± 0.3	2.3 ± 0.1	2.4 ± 0.3	2.2 ± 0.4	2.3 ± 0.3
P	.04	.07	.03	.04	.001

Abbreviation: SUV, standardized uptake value.
(*Adapted from* Bural GG, Torigian DA, Chamroonrat W, et al. Quantitative assessment of the atherosclerotic burden of the aorta by combined FDG-PET and CT image analysis: a new concept. Nucl Med Biol 2006;33:1037–43; with permission.)

Fig. 1. Assessment of changes in global metabolic activity of aortic atherosclerosis (atheroburden) with increasing age. (*Adapted from* Bural GG, Torigian DA, Chamroonrat W, et al. Quantitative assessment of the atherosclerotic burden of the aorta by combined FDG-PET and CT image analysis: a new concept. Nucl Med Biol 2006;33:1037–43; with permission.)
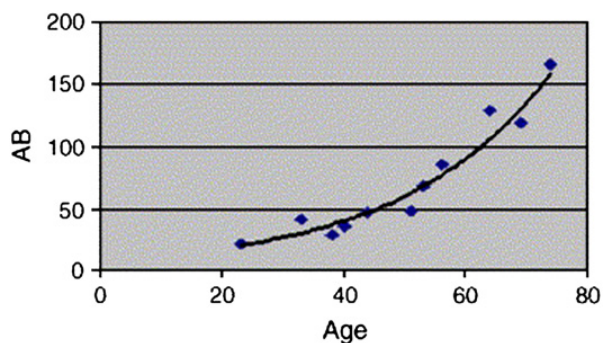
(n = 6) cancer. They concluded that the visual response score and *ΔTLG* are substantially correlated with other response parameters and are highly reproducible.

Advances in medical image segmentation within the context of quantitative PET imaging

Image segmentation has been employed in several clinical and research applications of quantitative PET imaging [5]. These include estimation of organ and tumor volumes as well as delineation of target treatment volumes in external radiotherapy, extraction of parameters of clinical relevance such as the left ventricular region in nuclear cardiology [6], automated ROI delineation of structures of interest in dynamic functional imaging [7], generation of functional images to highlight regions of similar temporal behavior (components) [8], determination of the attenuation map in emission tomography [9], anatomically guided image reconstruction and partial volume segmentation [10], and construction of voxel-based anthropomorphic phantoms based on high-resolution anatomical images [11].

One important application of this approach has been in the calculation of tissue metabolism of different brain components and MRI-guided partial volume correction in PET. **Fig. 2** shows a representative slice of a T2-weighted MR image through the brain and the corresponding segmentation results separately showing each tissue type including gray matter (GM), white matter (WM), and cerebrospinal fluid (CSF). MR images were first corrected for inhomogeneity and were subsequently standardized with regard to intensity before application of the segmentation algorithm. The mean intensity and standard deviation for each of GM,

Table 4: **Pre- and posttreatment assessment of Global Metabolic Burden (Volume × SUV) in patients with lymphoma**

Case	Pre Rx SUVmean	Post Rx SUVmean	% change	Pre Rx SUVmax	Post Rx SUVmax	% change	Pre Rx SUVmax	Post Rx SUVmax	% change	Pre Rx SUVmax	Post Rx SUVmax	% change
1	3.4	0	100	11.25	0	100	58	5	91	199	0	100
2	2.33	0.77	67	6.29	1.96	69	152	34	78	333	78	77
3	17	12	29	23	17.5	24	50	50	0	850	600	29

Abbreviations: post Rx, post-treatment; pre Rx, pretreatment; SUV, standardized uptake value.
(*Reprinted from* Basu S, Zaidi H, Houseni M, et al. Novel quantitative techniques for assessing regional and global function and structure based on modern imaging modalities: implications for normal variation, aging and diseased states. Semin Nucl Med 2007;37:223–39; with permission.)
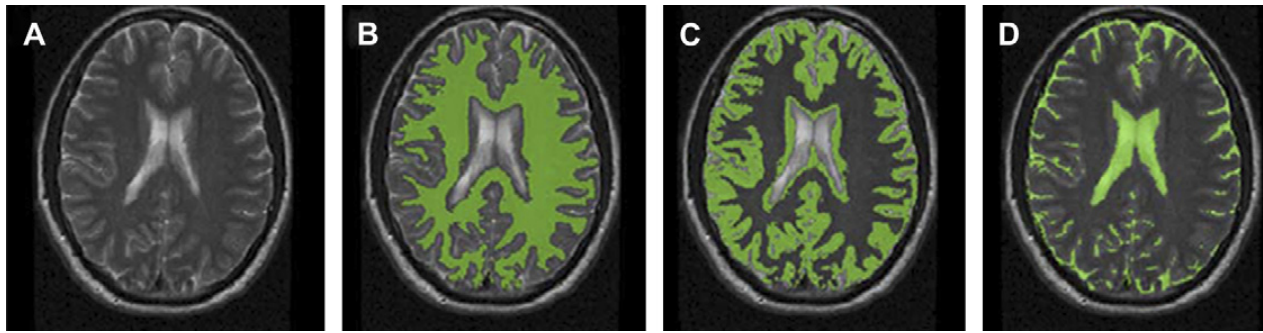
Fig. 2. Segmentation technique used to calculate SUV in GM, WM, and CSF. (*A*) Axial slice of intensity inhomogeneity corrected and intensity standardized T2-weighted image. (*B–D*) Color overlays on same axial T2-weighted image corresponding to segmented WM, GM, and CSF, respectively. (*Reprinted from* Basu S, Zaidi H, Houseni M, et al. Novel quantitative techniques for assessing regional and global function and structure based on modern imaging modalities: implications for normal variation, aging and diseased states. Semin Nucl Med 2007;37(3):223–39; with permission.)

WM, and CSF regions were subsequently determined from the training data set and are then fixed. A fuzzy connectedness framework was used for creating a brain intracranial mask, and the fuzzy membership value of each voxel in each brain tissue was estimated, and final segmentation of the brain tissues was simply performed via a maximum likelihood criterion as described by Zhuge and colleagues [12].

The same segmentation technique has also been employed in the lung parenchyma. Historically, segmentation of the lungs on CT scans has been a popular research area because of its usefulness in computer-based analysis of thoracic CT images and computer-aided diagnosis. A number of image segmentation approaches have been proposed and many of them have found applications in clinical settings. For example, the software system 3DVIEW-NIX [13] was used to segment the CT image of the lungs to obtain the left and the right lung. The steps were as follows: (1) The *Threshold* operation was used to segment the lung tissue from the rest of the CT image. (2) Subsequently, *Interactive2D* was used to manually remove the areas that were not a part of the lungs or were a part of the airway tree. (3) The mask that was produced covered only the lung area. Using *Interactive2D* once again, the left lung was removed and hence the mask for the right lung was obtained. (4) *Algebra* was used to obtain the left lung by subtracting the right lung mask from the entire lung mask. **Fig. 3** displays the segmentation results on a chest CT in one subject.

In PET imaging of cancer patients, image segmentation has a variety of important applications for tumor quantitation in staging, assessment of tumor response to therapy, and definition of target volumes for radiation therapy planning [14,15]. One such novel automated system was recently proposed for the segmentation of oncological PET data aiming at providing an accurate quantitative analysis tool [16]. The initial step involves Expectation Maximization (EM)-based mixture modeling using a k-means clustering procedure, which varies voxel order for initialization. A multiscale Markov model is then used to refine this segmentation by modeling spatial correlations between neighboring image voxels. Anthropomorphic phantom experiments were conducted for quantitative evaluation of the performance of the proposed segmentation algorithm. The comparison of actual tumor volumes to the volumes calculated using different segmentation methodologies including standard k-means, spatial-domain Markov Random Field Model (MRFM), and the new multiscale MRFM showed that the latter dramatically reduces the relative error to less than 8% for small lesions (7-mm radii) and less than 3.5% for larger lesions (9-mm radii). The analysis of the resulting segmentations of clinical oncologic PET data confirms that this method can successfully segment patient lesions. For problematic PET images (**Fig. 4**), this technique permits the identification of tumors situated very close to areas of nearby high normal physiological uptake.

To enhance lesion detectability, using similarity measures for analysis of dynamic oncological imaging to increase the contrast between normal tissues and lesions is a promising approach [17]. One such method, proposed originally for cardiac imaging is now being investigated for oncology PET studies. This uses the cross-y_B-energy operator, a nonlinear similarity measure that quantifies the interaction between two time-signals including their first and second derivatives [8]. Similarity measure between the time activity curve (TAC) of each pixel and the mean value of the TACs of a reference region of the dynamic image series is calculated, thereby
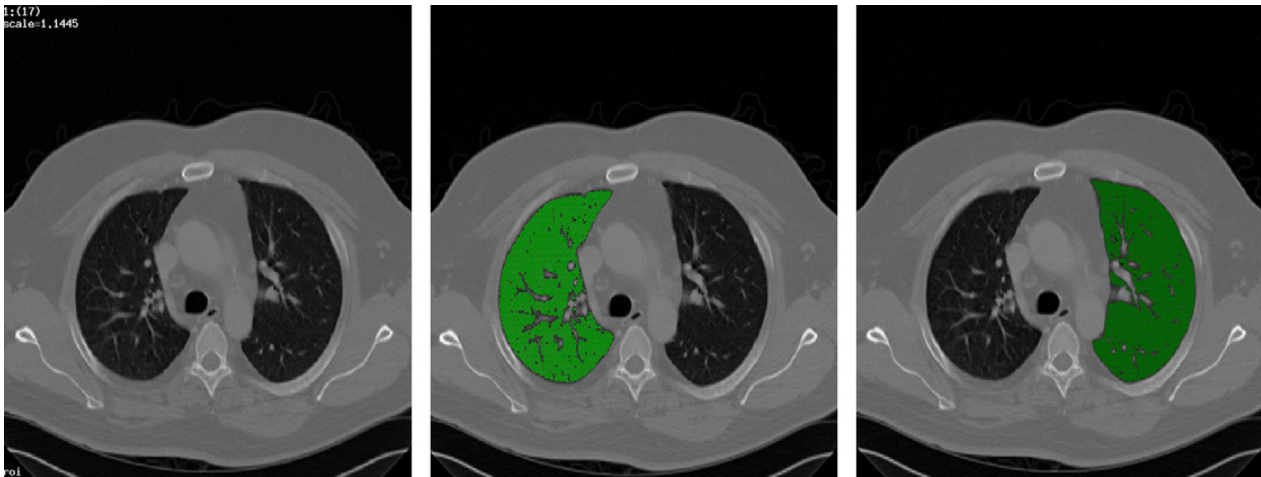
Fig. 3. Illustration of lung CT segmentation results. From left to right: original axial CT image, right lung segmentation, and left lung segmentation. (*Reprinted from* Basu S, Zaidi H, Houseni M, et al. Novel quantitative techniques for assessing regional and global function and structure based on modern imaging modalities: implications for normal variation, aging and diseased states. Semin Nucl Med 2007;37(3):223–39; with permission.)

generating images that demonstrate temporal changes in radioactive tracer distribution.

Principle of partial volume correction of standardized uptake value for the purpose of calculating global metabolic activity

The partial volume effect is one of the important technical constraints for accurate quantitation with PET, mostly related to the scanner resolution (see the article by Rousset and colleagues elsewhere in this issue). There is growing concern with regard to partial volume effect correction on the quantification procedure in FDG-PET studies in small lesions [18]. This effect is also a problem in other imaging techniques including single-photon emission computed tomography and structural imaging, when small objects (compared with the imaging system's spatial resolution) are examined. Many investigators have addressed this effect in brain PET studies [10,19–25], where the major concern is to measure the exact concentration of the tracers such as FDG in the brain. In practice, the actual spatial resolution of the reconstructed PET images is substantially less than that specified by phantom studies that are typically at best 4 mm using state of the art clinical PET scanners. This limited spatial resolution leads to an inaccurate measurement of the true concentration of the radiotracer in lesions less than 2 to 3 times the spatial resolution of the PET scanner as defined by the full-width at half-maximum (FWHM) of a point-spread function. One method to correct for the PVE is to use the lesion size as determined by anatomic imaging modalities as the basis for the calculation of the correct SUV [26,27].

Fig. 4. Illustration of the automated segmentation procedure for PET. From left to right: original clinical image, resultant segmentation (eight segments) using traditional MRFM, and resultant segmentation using multiscale MRFM. (*Adapted from* Montgomery D, Amira A, Zaidi H. Fully automated segmentation of oncological PET volumes using a combined multiscale and statistical model. Med Phys 2007;34:722–36; with permission.)

This represents an essential step in calculating the global metabolic activity.

Summary

In the near future, it is likely that highly sophisticated methodologies and software for accurate quantitative analysis will become widely available in clinical settings and no longer restricted to large research groups where highly skilled technical staff is available. The motivation of vendors to develop and incorporate advanced software for quantitative analysis is triggered by interest and demand from the clinicians as end users. It is expected that this will happen shortly so that the estimation of global metabolic activity and other quantitative parameters will become routine in the practice of clinical PET imaging.

References

[1] Alavi A, Newberg AB, Souder E, et al. Quantitative analysis of PET and MRI data in normal aging and Alzheimer's disease: atrophy weighted total brain metabolism and absolute whole brain metabolism as reliable discriminators. J Nucl Med 1993;34:1681–7.

[2] Keyes J. SUV: standard uptake value or silly useless value? J Nucl Med 1995;36:1836–9.

[3] Bural GG, Torigian DA, Chamroonrat W, et al. Quantitative assessment of the atherosclerotic burden of the aorta by combined FDG-PET and CT image analysis: a new concept. Nucl Med Biol 2006;33:1037–43.

[4] Larson SM, Erdi Y, Akhurst T, et al. Tumor treatment response based on visual and quantitative changes in global tumor glycolysis using PET-FDG imaging. The visual response score and the change in total lesion glycolysis. Clin Positron Imaging 1999;2:159–71.

[5] Quantitative analysis in nuclear medicine imaging. In: Zaidi H, editor. New York: Springer; 2006. p. 564.

[6] Behloul F, Lelieveldt BP, Boudraa A, et al. Neuro-fuzzy systems for computer-aided myocardial viability assessment. IEEE Trans Med Imaging 2001;20:1302–13.

[7] Wong K-P, Dagan F, Meikle SR, et al. Segmentation of dynamic PET images using cluster analysis. IEEE Trans Nucl Sci 2002;49:200–7.

[8] Boudraa A, Cexus J-C, Zaidi H. Functional segmentation of dynamic nuclear medicine images by cross-PsiB energy operator. Comput Methods Programs Biomed 2006;84:148–54.

[9] Zaidi H, Hasegawa BH. Determination of the attenuation map in emission tomography. J Nucl Med 2003;44:291–315.

[10] Baete K, Nuyts J, Laere KV, et al. Evaluation of anatomy based reconstruction for partial volume correction in brain FDG-PET. Neuroimage 2004; 23:305–17.

[11] Zaidi H, Xu XG. Computational anthropomorphic models of the human anatomy: the path to realistic Monte Carlo modeling in medical imaging. Annu Rev Biomed Eng 2007;9: 471–500.

[12] Zhuge Y, Liu J, Udupa JK. Membership-based multiprotocol MR brain image segmentation. Medical Imaging 2003: Image Processing, San Diego, CA, USA, 2003/05/16/, 2003;5032:1572–9.

[13] Udupa JK, Odhner D, Samarasekera S, et al. 3DVIEWNIX: an open, transportable, multi-dimensional, multimodality, multiparametric imaging software system. Medical Imaging 1994: Image Capture, Formatting, and Display, Newport Beach, CA, USA, 1994/05/01/, 1994;2164: 58–73.

[14] Paulino AC, Thorstad WL, Fox T. Role of fusion in radiotherapy treatment planning. Semin Nucl Med 2003;33:238–43.

[15] Gregoire V, Haustermans K, Geets X, et al. PET-based treatment planning in radiotherapy: a new standard? J Nucl Med 2007;48:68S–77S.

[16] Montgomery D, Amira A, Zaidi H. Fully automated segmentation of oncological PET volumes using a combined multiscale and statistical model. Med Phys 2007;34:722–36.

[17] Thireou T, Kontaxakis G, Strauss LG, et al. Feasibility study of the use of similarity maps in the evaluation of oncological dynamic positron emission tomography images. Med Biol Eng Comput 2005; 43:23–32.

[18] Soret M, Bacharach SL, Buvat I. Partial-volume effect in PET tumor imaging. J Nucl Med 2007; 48:932–45.

[19] Tanna NK, Kohn MI, Horwich DN, et al. Analysis of brain and cerebrospinal fluid volumes with MR imaging: impact on PET data correction for atrophy. Part II. Aging and Alzheimer dementia. Radiology 1991;178:123–30.

[20] Chawluk J, Alavi A, Dann R, et al. Positron emission tomography in aging and dementia: effect of cerebral atrophy. J Nucl Med 1987;28:431–7.

[21] Rousset OG, Ma Y, Evans AC. Correction for partial volume effects in PET: principle and validation. J Nucl Med 1998;39:904–11.

[22] Frouin V, Comtat C, Reilhac A, et al. Correction of partial volume effect for PET striatal imaging: fast implementation and study of robustness. J Nucl Med 2002;43:1715–26.

[23] Aston JA, Cunningham VJ, Asselin MC, et al. Positron emission tomography partial volume correction: estimation and algorithms. J Cereb Blood Flow Metab 2002;22:1019–34.

[24] Quarantelli M, Berkouk K, Prinster A, et al. Integrated software for the analysis of brain PET/SPECT studies with partial-volume-effect correction. J Nucl Med 2004;45:192–201.

[25] Zaidi H, Ruest T, Schoenahl F, et al. Comparative evaluation of statistical brain MR image segmentation algorithms and their impact on partial volume effect correction in PET. Neuroimage 2006;32: 1591–607.

[26] Hickeson M, Yun M, Matthies A, et al. Use of a corrected standardized uptake value based on the lesion size on CT permits accurate characterization of lung nodules on FDG-PET. Eur J Nucl Med Mol Imaging 2002;29: 1639–47.

[27] Basu S, Zaidi H, Houseni M, et al. Novel quantitative techniques for assessing regional and global function and structure based on modern imaging modalities: implications for normal variation, aging and diseased states. Semin Nucl Med 2007;37:223–39.